




Photo-Seebeck study of amorphous germanium–tellurium-oxide films

A. Baset Gholizadeh¹, Alex S. Walton², Richard Smith³, Jonathan England³, Christopher Craig⁴, Dan Hewak⁴, and Richard J. Curry^{1,*} 

¹Department of Electrical and Electronic Engineering, Photon Science Institute, University of Manchester, Manchester M13 9PL, UK

²Department of Chemistry, Photon Science Institute, University of Manchester, Manchester M13 9PL, UK

³Ion Beam Centre, University of Surrey, Guildford, Surrey GU2 7XH, UK

⁴Optoelectronics Research Centre, University of Southampton, Southampton SO17 1BJ, UK

Received: 2 October 2020

Accepted: 16 October 2020

Published online:
29 October 2020

© The Author(s) 2020

ABSTRACT

The measurement of the Seebeck coefficient of thin film (100 nm) amorphous germanium telluride containing ~ 31% oxygen under dark conditions and when exposed to monochromatic light in the 400 nm to 1800 nm wavelength region is reported. Exposure of the films to light is found to reduce the absolute value of the Seebeck coefficient compared to that measured in the dark. Furthermore, the magnitude of this reduction displays a distinctive spectral dependence over the wavelength range covered. The observed behaviour suggests that these measurements provide a method determining the optical bandgap of thin amorphous chalcogenide films. Further analysis of the data, along with that of X-ray photoelectron spectroscopy and photoconductivity studies, is used to determine the presence of sub-bandgap defect states and their role in determining the optical response of the Seebeck coefficient.

1 Introduction

Amorphous semiconductors, and chalcogenides in particular, are interesting materials that display a broad range of physical phenomena resulting in wide-ranging studies of their fundamental properties and their application [1, 2]. Amorphous germanium telluride (a-GeTe) is of particular interest as it forms the basis of Ge–Sb–Te alloy systems that have been exploited in phase-change memory (PCM) applications [3, 4]. a-GeTe has a crystallisation temperature > 150 °C and can be reversibly switched

between the amorphous and crystalline state at high speed [5]. Despite the significant research attention this and other applications have attracted, a full understanding the electronic and thermoelectric properties of these materials remains a challenge due to their non-crystalline structure. Recently the role of oxidation in a-GeTe has been studied, demonstrating its role in the detrimental modification of the crystallization dynamics and chemistry of thin films [6–10].

Electronic and optical studies [11, 12], including photoconductivity [13], have resulted in a

Address correspondence to E-mail: Richard.Curry@manchester.ac.uk

continuously evolving understanding of the electronic structure of a-GeTe thin films. Evidence supports the presence of a bandgap (at 300 K) of ~ 0.75 eV [14] to 0.85 eV [15], a donor state at ~ 0.25 eV above the valence band, and one or more acceptor states at ~ 0.35 eV below the conduction band. Modelling of a-GeTe using density functional theory (DFT) approaches has also led to the prediction of mid-gap states upon melt quenching, though with a narrower bandgap (~ 0.4 eV) [16]. It was further suggested that the mid-gap state is directly associated with the presence of homopolar Ge–Ge bonding, itself linked to tetrahedral Ge bonding. Thermoelectric power studies of bulk GeTe have yielded a Seebeck coefficient (S) value of ~ 35 to $80 \mu\text{V K}^{-1}$ at 300 K [17–21]. In contrast, reports for measurement of S in a-GeTe thin films by Bahl [22] (200 nm), Dutsyak [23] ($< 1 \mu\text{m}$ thick) and Hughes [24] (100 nm) yielded much higher values of $\sim 800 \mu\text{V K}^{-1}$, with measurement of crystalline GeTe yielding values similar to those reported for bulk sample [17]. However, the study of 500 nm annealed polycrystalline (rhombohedral) GeTe films yielded a value of $S \sim 80 \mu\text{V K}^{-1}$ [25] similar to the bulk. Interestingly, the study of hot-pressed GeTe rods formed from $< 200 \mu\text{m}$ diameter particles yielded a values of $S \sim 170 \mu\text{V K}^{-1}$ at 300 K. In all of the above it is likely that some of the variation in reported properties between studies may be due to the effects of oxidation.

The measurement of the Seebeck coefficient, under dark conditions (S_{dark}), can be used to experimentally determine the majority carrier type of a semiconductor, including amorphous systems for which the Hall effect can provide anomalous results [26–28]. As indicated above the positive values of S reported lead to the conclusion that a-GeTe is a p-type semiconductor in common with the majority of chalcogenides. A general understanding of p-type conductivity in amorphous chalcogenides is given by considering the presence of lone pair electrons leading to the formation of defects and valence alternation pairs (VAPs) that ultimately result in an excess of holes in the valence band [29].

Though it is generally the case that S is measured under dark conditions, S can also be strongly affected by additional factors including by the absorption of light [30–34]. Although Mondal et al. [35] reported an increase in the magnitude of S upon light exposure (S_{light}) in Pb_2CrO_5 , in general it is found that

illumination of a sample with light reduces the magnitude of S such that $|S_{\text{dark}}| > |S_{\text{light}}|$. This reduction can in some cases be large enough that the sign of S_{dark} and S_{light} may differ and the majority carrier type is reversed [31].

Here we report the measurement of S_{dark} and S_{light} of ~ 100 nm oxidised a-GeTe films as a function of optical excitation wavelength across the visible and near-IR spectral region. It is found that the variation between S_{dark} and S_{light} reveals a dependency of photon energy that also includes a sub-electronic bandgap (E_g) behaviour.

2 Experimental procedure

a-GeTe thin films of 100 nm nominal thickness were sputtered from a target of composition $\text{Ge}_{50}\text{Te}_{50}$ (purchased from Testbourne) onto high resistivity ($> 10^{12} \text{cm}\Omega^{-1}$) 1 mm thick fused silica substrates using a Kurt J. Lesker Nano 38 Sputter thin film deposition system. The substrate was inserted at room temperature with less than a 10°C increase observed during deposition. High purity argon was used as the sputtering gas and the distance between the target and the substrate was 150 mm. The films were deposited using a deposition power 60 W, a DC bias of 214 V, and whilst maintaining a base pressure of $\sim 3.4 \times 10^{-3}$ mbar with an argon gas flow of 20 SCCM. The film thickness was measured on a KLS Tencor P16 Stylus Profiler and determined to be 100 ± 5 nm.

To enable electrical measurements Cr (100 nm)/Mo (50 nm) top electrodes were defined by sputtering through a shadow mask with 2 mm diameter circle apertures. Cr was sputtered (1000 W) for 15 min followed by Mo at the same power for 5 min. The ohmic nature of the contacts was confirmed in subsequent electrical measurement (in the dark), displaying linear current–voltage (I – V) characteristics (Fig. 1), yielding a measured conductivity of $5.6425 \times 10^{-10} \pm 1.74 \times 10^{-11} \text{S cm}^{-1}$. It is immediately noted that this value is six orders of magnitude smaller than that typically reported for a-GeTe [9] and three orders smaller than that reported for similar film by Hughes et al. [24]. As such it is clearly evident that modification of the deposited film had taken place during or following its deposition, noting that the films were transferred and stored under dark

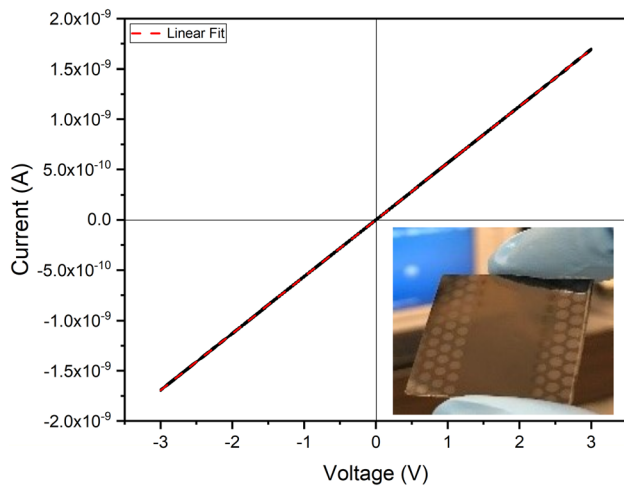


Fig. 1 I - V scan of a-GeTe film obtained using adjacent Cr (100 nm)/Mo (50 nm) electrodes. The distance between the measured electrodes was ~ 1.8 cm. Inset is an image of the a-GeTe sample

but ambient atmosphere conditions hence oxidation was likely to have occurred.

Compositional analysis Rutherford backscattering spectrometry (RBS) measurements were performed by the EPSRC National Ion Beam Centre that confirmed the presence of oxygen throughout the films, yielding a film composition of composed of Ge = $34.4\% \pm 0.3$ and Te = $33.8\% \pm 0.2$ and O = 31.8% (Fig. 2 and Table 1). A ~ 2 mm diameter 2 meV ^4He ion beam was used with a charge collection of 10 μC . Backscattered He ions were simultaneously collected at Cornell (detector A) and IBM (detector B) geometries for scattering angles of 173.2° and 148.6° , respectively.

Spectra were analysed using SIMNRA assuming Rutherford cross sections throughout with the best fits being determined by eye [36]. No pile up correction was applied. The spectra were calibrated for energy by measuring a Au/NiCu/SiO₂/Si standard sample and the solid angle charge product was internally calibrated for each spectrum by fitting to the Si in the SiO₂ substrate. The substrate model used in the SIMNRA fit was kept simple by assuming a single layer of Ge_xTe_yO_z on a SiO₂ substrate; where the fitted peak representing the O in the Ge_xTe_yO_z film was lower than the measured data, the O concentration was scaled by the ratio of the measured to fitted peak areas. For the Cornell geometry, the O in the substrate and a simple background subtraction based on the Si signal could be applied. For the IBM geometry, the two O signals overlapped and so a more complex background was subtracted from the peak representing the O in the Ge_xTe_yO_z film after fitting a polynomial to the O edge below and Si signal above the peak. It is usual to determine a single best sample composition to give the best fits to the spectra at both geometries simultaneously. In this case, independent fits (Table 1) were made so that their comparisons could give an indication of the absolute uncertainty in the O concentration. Errors quoted in the table are from counting statistics ($1/\sqrt{\text{counts}}$) alone. The differences between the calculated values is larger than these errors demonstrating that there are systematic errors (for example, accuracy of stopping powers or accuracy of fit) that are hard to estimate from first principles. Interestingly the RBS

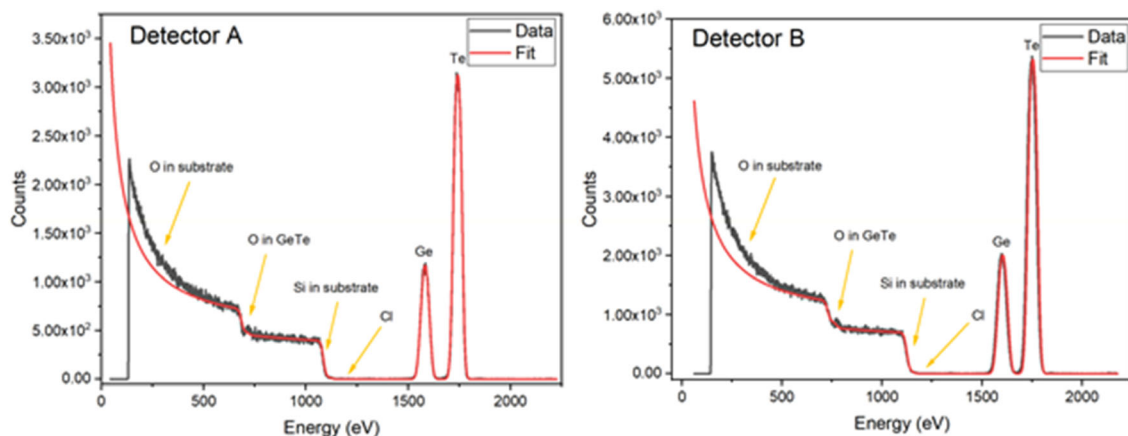


Fig. 2 RBS spectra of 100 nm GeTe film on SiO₂. The left (detector A) spectrum is acquired using the Cornell geometry and the right spectrum (detector B) collected in the IBM geometry

Table 1 Elemental composition of a-GeTe film

Element	Cornell (173.2°)		IBM (148.6°)		Composition (at%)
	TFU	GeTe ratio	TFU	GeTe ratio	
Ge	128.1 (6)	50.5	125.8 (4)	50.3	34.4 (3)
Te	125.4 (3)	49.5	124.1 (2)	49.7	33.8 (1)
O	117 (1)		118 (2)		31.8 (4)

1 TFU = 1×10^{15} atoms/cm²

analysis was also able to detect trace amounts of residual Cl on the surface of the fused silica substrate. Analysis of the spectra collected above and in-plane yielded the film composition given in Table 1.

XPS analysis was used to determine the value of E_f and the top of the valence band energy level for the films and presented in Fig. 3 [37]. The samples were mounted on a metal plate, using silver epoxy to provide electrical contact between the plate and the a-GeTe film. The sample was then biased to -10 V to ensure that the secondary electron tail could be observed. The sample was Ar^+_{3000} sputtered to remove any carbonaceous surface material and oxide layer prior to measurement. It is noted that the O 1s peak remained following sputtering confirming, in agreement with the RBS analysis, the presence of oxygen within the film. A Fermi edge scan on the metal contact pad (which was grounded to the sample plate) was undertaken and used to calibrate the energy scale.

The a-GeTe Fermi level was determined to be $E_f = -4.05$ eV by taking the difference of the excitation energy (1486.6 eV) and the secondary electron tail ($\sim 1482.55 \pm 0.1$ eV) which is presented in Fig. 4. The a-GeTe valence band maximum (VBM) with respect to the Fermi energy was found to be 0.16 ± 0.1 eV yielding a valence band energy of $E_v = -4.21$ eV.

Seebeck measurements were undertaken within a bespoke vacuum chamber with a base pressure of $\sim 2 \times 10^{-6}$ mbar. The chamber also acted as a faraday cage with electrical (triax and type-K thermocouple), optical fibre and sealed liquid/gas feed-throughs enabling electrical measurement, optical excitation, and cooling of the sample under test. A schematic of the system and control hierarchy is provided in Fig. 5.

The optical fibre vacuum feedthrough enabled variable wavelength optical excitation of the sample, ensuring no light exposure of the metal contacts. A

stable temperature gradient was established across the sample by passing a controlled flow of cooled N_2 gas through a cooling block and Peltier heating of a second separated block across which the sample was placed, ensuring that the temperature did not exceed 100 °C. This is well below the crystallisation temperature of oxidized a-GeTe films of ~ 180 °C [6]. The sample temperature was measured before and following each electrical measurement by lowering two (small) type-K thermocouples probes onto the sample at the opposing points of electrical measurement. Studies were undertaken at four different values of $\Delta T = 15, 27, 41$ and 58 °C. The electrical measurements were performed using a Keysight B1500A equipped with a high-resolution source measure unit (HRSMU). Illumination of the sample was enabled by coupling the monochromated (via Bentham TMc300 monochromator) output of a tungsten halogen source (Osram 64623 HLX) into a one-metre multimode optical fibre (Thorlabs M37L01), through a vacuum optical feed-through (Thorlabs V2H6S) and the internal fibre (MV12L05) directed to provide close illumination of the sample under test. High-quality long pass filters were used to ensure the rejection of second order reflections, and neutral density filters used to control light intensity. By adjustment of the fibre tip-to-sample separation the diameter of the incident light spot on the sample was controlled to maximise the exposure area whilst minimising the risk of direct or scattered light being incident on the electrical probes. This was undertaken to prevent any photovoltaic effect occurring during optical measurements (e.g. in the case of Schottky contacts being present). All measurements of S_{light} were undertaken starting from the lowest energy (longest wavelength), with continuous monitoring of the electrical signal to ensure that electrical equilibrium had been reached following each change of wavelength, prior to measurements to determine S_{light} . Conductivity and photoconductivity

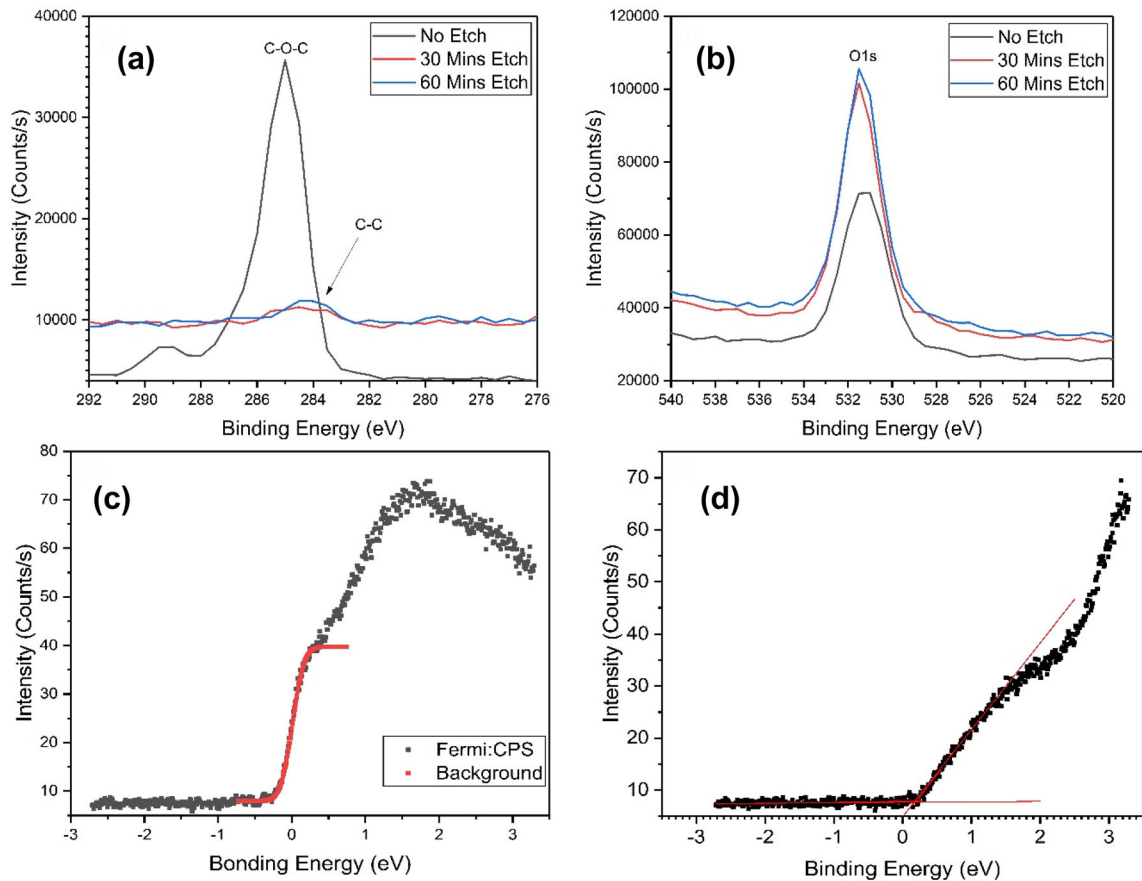


Fig. 3 XPS spectra of 100 nm a-GeTe film on SiO₂. **a** C 1s region, showing the near-complete removal of carbon contamination from the surface of the GeTe film after Ar⁺₃₀₀₀ sputtering, **b** O 1s spectra showing that oxygen remains even after extensive sputtering, indicating its presence throughout the a-GeTe film.

c Valence band region of the metal contact pad, showing the Fermi edge fitted with a Fermi–Dirac function. **d** Valence band region of the a-GeTe film, showing the valence band onset fitted using the linear intercepts method

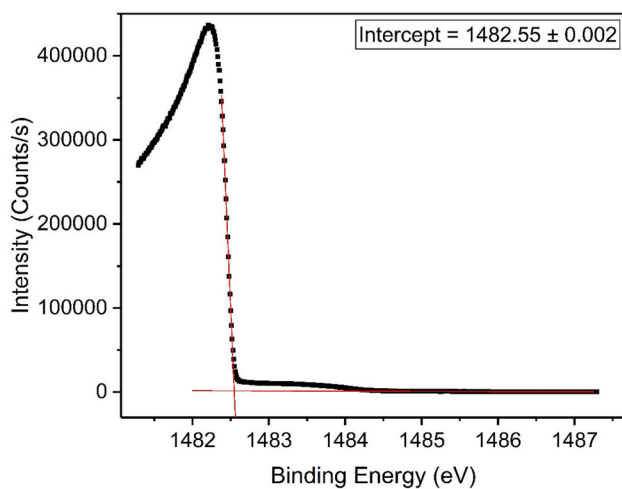


Fig. 4 Secondary electron tails detected from the a-GeTe film using XPS

measurements utilised the above described setup and a two-probe measurement technique. This allows direct comparison of the results obtained in each case. In this method, the measured value of conductance was normalised by the distance between the two electrical contacts (1.8 ± 0.1 cm) through which the current flows. In the case of some amorphous semiconductors, a high current may lead to a phase change effect due to Joule heating, causing a transition of the film from an amorphous to crystalline structure. To limit this risk conductivity measurements were obtained by sweeping a small voltage range from -3 to 3 V; in all cases no behaviour indicative of a phase change was observed.

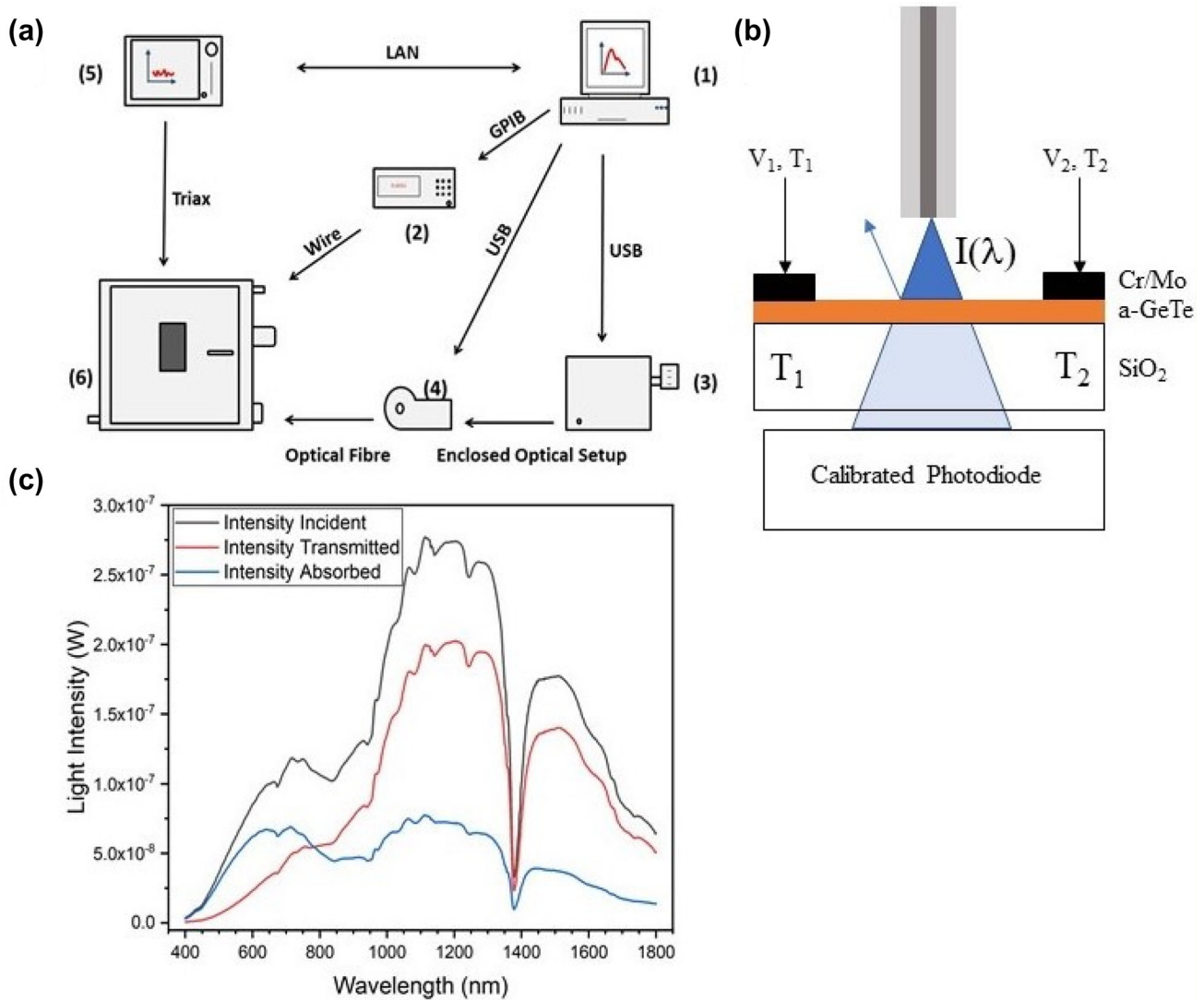


Fig. 5 a Schematic of the system and control hierarchy. b Schematic of the Seebeck system and measurement of the transmitted light intensity. c Intensity of incident, transmitted and absorbed light

3 Results

The Seebeck coefficient in p-type semiconductor in the dark is described by [38]:

$$S_{\text{dark}} = \frac{\Delta V}{\Delta T} = + \frac{k_B}{q} \left[\frac{E_f - E_v}{k_B T} + r + \frac{5}{2} \right], \tag{1}$$

where k_B is the Boltzmann constant, q is the electron charge, E_f is the Fermi level, E_v is position of the valence band, and T is temperature. The parameter r is a scattering parameter equal to $3/2$ for impurity scattering and $-3/2$ for lattice scattering of carriers. Under light illumination, the Seebeck coefficient may be modified by the excitation of charge carriers across the bandgap, or to and from trapped states. In such

circumstances both electrons and holes may contribute to the measured value of S_{light} . Assuming that carrier excitation due to light absorption occurs throughout the thin film, true for the 100 nm films used, the modified conductivity, σ_{light} , is given as:

$$\sigma_{\text{light}} = \sigma_e + \sigma_h, \tag{2}$$

where $\sigma_{e(h)}$ is the electron (hole) conductivity. As a result of the modified conductivity the Seebeck coefficient is now obtained as:

$$S_{\text{light}} = \frac{\sigma_e S_e + \sigma_h S_h}{\sigma_e + \sigma_h}. \tag{3}$$

The measured value of S_{dark} was obtained to be $0.434 \pm 0.011 \text{ mV K}^{-1}$, confirming the p-type nature of the film, Fig. 6.

The value obtained is of the same order of magnitude to that reported for a-GeTe films which were deposited in a similar way [18–20] though reduced by approximately a factor of 2. This indicates that the oxidised a-GeTe films remain amorphous, whereas polycrystalline films display a value of S_{dark} that is at least an order of magnitude lower. Using Eq. 1 with the measured values of E_f and E_v from XPS studies (assuming lattice scattering dominates [21]) yields an expected value of $S_{\text{dark,calc}} = 0.6 \text{ mV K}^{-1}$ at 300 K, again of the same order of magnitude as the measured value. Conversely, use of the measured value of S_{dark} to calculate the expected Fermi level results in an underestimate of $\sim 60 \text{ meV}$ in comparison to that measured using XPS.

Upon illumination with monochromatic light to measure S_{light} a wavelength dependent reduction in the Seebeck coefficient compared to S_{dark} is observed, Fig. 7. This reduction in the Seebeck coefficient upon light illumination infers that the Fermi level within the a-GeTe film is increased as a result of exposure, i.e. the film becomes less p-type. It was confirmed that upon returning the film to dark conditions that S_{dark} was recovered. However, this process is not immediate but required many hours to complete implying long-lived (deep) charge carrier trap states may be involved in the observed behaviour. It is

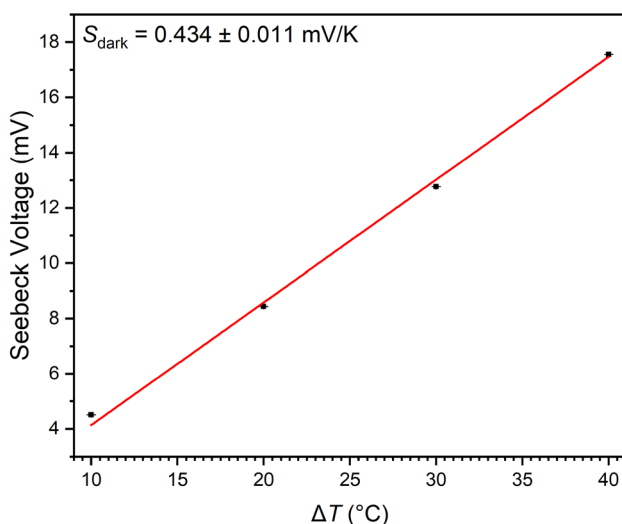


Fig. 6 Seebeck coefficient of a-GeTe film determined using the measured Seebeck voltage as a function of the applied temperature gradient

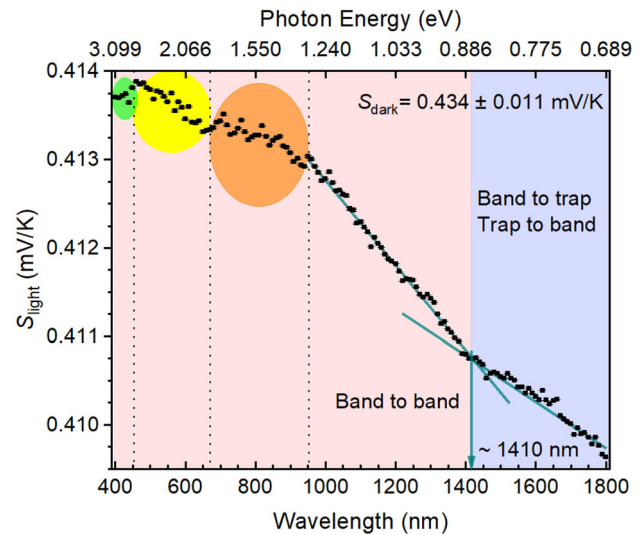


Fig. 7 Seebeck coefficient of a-GeTe obtained as a function of monochromatic light excitation at wavelengths between 400 and 1800 nm. The potential optical bandgap is indicated with a green arrow (Color figure online)

noted that the wavelength dependence, $S_{\text{light}}(\lambda)$, extends across the entire spectral region accessible (400 nm to 1800 nm) and surprisingly shows the greatest reduction from S_{dark} at the lowest photon energies.

Inspection of the variation of $S_{\text{light}}(\lambda)$ in Fig. 7 reveals distinctive regions of similar behaviour. Upon initial exposure to light at 1800 nm (0.68 eV), $S_{\text{light}}(1800 \text{ nm})$ is $\sim 0.025 \text{ mV/K}$ lower than S_{dark} corresponding to a $\sim 6\%$ decrease. $S_{\text{light}}(\lambda)$ is seen to increase approximately linearly with reducing wavelength to $\sim 1410 \text{ nm}$ (0.88 eV). As the wavelength is reduced further, $S_{\text{light}}(\lambda)$ continues to increase linearly but at a greater rate up until $\sim 970 \text{ nm}$ (1.28 eV). The change in gradient of $S_{\text{light}}(\lambda)$ at 0.88 eV is slightly above the reported optical bandgap of a-GeTe of $\sim 0.75 \text{ eV}$ [8] to 0.85 eV [11]. This is in line with a widening of the bandgap upon oxidation, which is well-known to occur when chalcogenide glasses are oxygen doped.

At energies below the optical bandgap the magnitude of $S_{\text{light}}(\lambda)$ must be governed by the interaction of photons with charge carriers within, or excited to, sub-bandgap charge states (e.g. trap-to-band and band-to-trap transitions). Previous studies of photoconductivity have also revealed a sub-bandgap response (down to photon energies of 0.2 eV) at room temperature which reduces with temperature in line with the observed behaviour [13]. Similarly,

Longeaud et al. found evidence of acceptor states at energies of 0.37 eV and 0.41 eV above the VB and a donor state at 0.26 eV below the CB [14]. These, combined with the presence of VB and CB tail states with Urbach energies of 32 meV and 59 meV, respectively, provide a clear rationale to expect a sub-bandgap photo-Seebeck response.

The increase in the sensitivity of $S_{\text{light}}(\lambda)$ to light exposure at energies above 0.88 eV is in alignment with the increase in the density of states (DOS) at the valence band edge, and the ability to optically excite valence electrons across the bandgap, E_g . A value of E_g is therefore tentatively assigned as $E_g = 0.88$ eV on the basis of these photo-Seebeck measurements alone. Attempts to directly measure the optical band edge of the a-GeTe films via both absorption and photothermal deflection spectroscopy proved unsuccessful due to the thinness of the films.

As the excitation wavelength is reduced further from ~ 970 to 400 nm $S_{\text{light}}(\lambda)$ displays three further regions of behaviour, all of which show a reduced gradient to that observed in lower energy (higher wavelength) excitation regions. The initial reduction of the energy dependence of $S_{\text{light}}(\lambda)$ at ~ 970 nm (1.27 eV) coincides with the reported onset of saturation of optical absorption in 800 nm a-GeTe films [14]. There then follows an increase in this dependence over the region from 620 nm (2.0 eV) to 450 nm (2.75 eV) which coincides with the reported peaks in binding energy obtained from valence band XPS studies [39, 40]. Finally, at the highest energies available (below 2.75 eV) the dependence of $S_{\text{light}}(\lambda)$ on wavelength appears to disappear, and the reduction from S_{dark} is at its smallest.

To provide further information on the photogenerated processes that result in the observed behaviour of $S_{\text{light}}(\lambda)$ in Fig. 7 the photo-Seebeck voltage, $V_{\text{light}}(\lambda)$, can be studied. Figure 8 presents $V_{\text{light}}(\lambda)$ as a function of excitation wavelength for $\Delta T = 15, 27, 41$ and 58 °C.

To correct for the variation in light intensity with wavelength $V_{\text{light}}(\lambda)$ is normalized by the number of photons absorbed at each wavelength (Fig. 5c). The prominent peak appearing at ~ 1380 nm is an artefact of the normalization originating from the strong optical fibre attenuation around this band (due to hydroxyl groups, Fig. 5c). From Fig. 8 it is clearly observed that the variation of $V_{\text{light}}(\lambda)$ either side of E_g (~ 1410 nm, 0.88 eV) is different. Below E_g there is evidence, in the form of ‘shoulders’, of optically

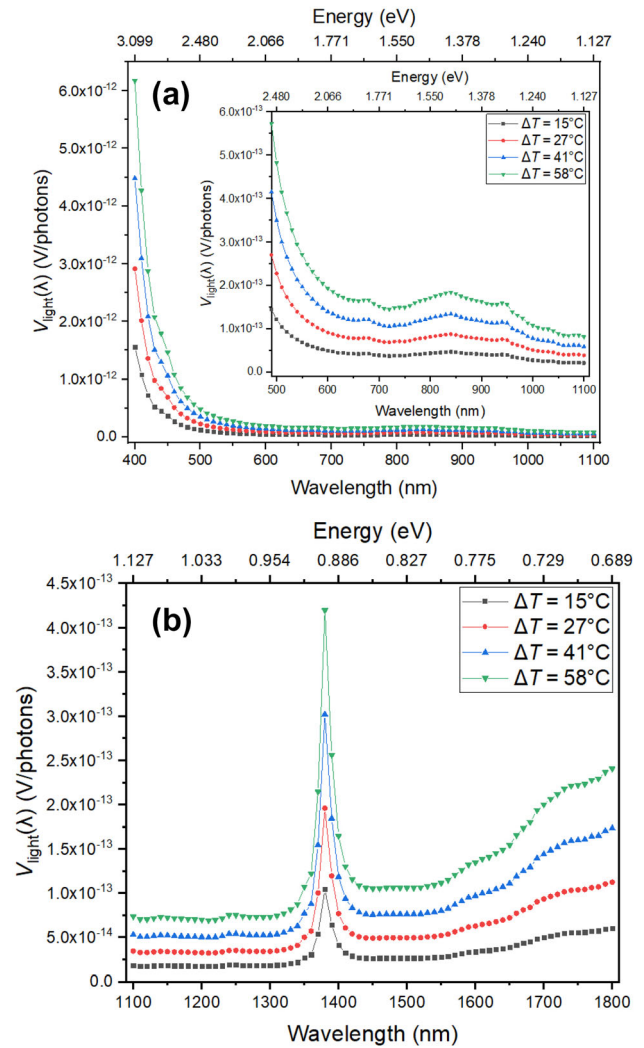


Fig. 8 Measured Seebeck voltage normalised by the number of absorbed photons. **a** Under excitation at wavelengths between 400 and 1100 nm and **b** between 1100 and 1800 nm. The narrow peak at ~ 1380 nm is an experimental artefact

induced transitions centred at ~ 1600 nm (0.78 eV) and ~ 1700 nm (0.73 eV), corresponding to a transition energy of ~ 0.1 eV and ~ 0.15 eV below E_g . Previous modulated photocurrent (MPC) and PDS studies have indicated that both the valence and conduction band display extended tails with characteristic energies of 0.33 eV and 0.6 eV, respectively [14]. Furthermore, to accurately reproduce the DOS obtained via MPC measurements, an additional donor state was required with an energy of 0.26 eV above the valence band. An additional pair of acceptor states with energies of 0.37 eV and 0.41 eV above the valence band were also included to obtain fits to PDS studies and pin the dark Fermi level at the

experimental value (0.31 eV). The energy difference between the reported donor and two acceptor states is 0.11 eV and 0.15 eV matching that of the transition energy of the observed peaks in $V_{\text{light}}(\lambda)$. As such the increase in $V_{\text{light}}(\lambda)$ below E_g provides a direct experimental observation that would support the presence of these states.

Turning attention to the behaviour of $V_{\text{light}}(\lambda)$ at energies above E_g it is seen that whilst there is an increase in $V_{\text{light}}(\lambda)$ with ΔT , no evidence of any wavelength dependence is observed as the excitation wavelength is decreased from ~ 1410 to 1100 nm (1.13 eV) (Fig. 8). Excitation in the 1100 nm to 470 nm region does then result in the re-emergence of the dependence of $V_{\text{light}}(\lambda)$ on wavelength. Inspection of $V_{\text{light}}(\lambda)$ in the region of ~ 1100 nm to ~ 700 nm shows the presence of a broad peak with its maximum at ~ 800 nm, with an accompanying small (reproducible) feature at ~ 950 nm. This broad peak in $V_{\text{light}}(\lambda)$ coincides with the change in the dependence of $S_{\text{light}}(\lambda)$ at ~ 950 nm (highlighted in orange, Fig. 7). Reducing the excitation wavelength further from ~ 700 to 600 nm reveals the presence of a further peak in $V_{\text{light}}(\lambda)$ at ~ 675 nm, which again corresponds to the change in the dependence of $S_{\text{light}}(\lambda)$ seen at this wavelength (highlighted yellow, Fig. 7). At excitation wavelengths below 600 nm $V_{\text{light}}(\lambda)$ then begins to rapidly increase with a evidence of a further feature centred at ~ 440 nm, leading to the final change in dependence of $S_{\text{light}}(\lambda)$ on wavelength (highlighted green, Fig. 7).

As discussed above, any modification of the Seebeck coefficient under illumination is related to the generation of excited carriers yielding an excited hole (electron) population of magnitude Δp ($= \Delta n$). Δp should be proportional to the incident light intensity, $I_0(\lambda)$, for low excitation powers and thus as $I_0(\lambda)$ is reduced $S_{\text{light}}(\lambda)$ should approach S_{dark} . Figure 9 shows $S_{\text{light}}(\lambda)$ as a function of incident light power, obtained individually for selected values of λ , and it is observed that as $I_0(\lambda)$ is reduced S_{dark} is approached.

The value of 100% in Fig. 9 corresponds to no attenuation of the monochromatic light, as was used in undertaking the measurements $S_{\text{light}}(\lambda)$ at 100% light intensity. We note that the values of $S_{\text{light}}(\lambda)$ in Fig. 9 are lower than those presented in Fig. 7 as a result of prior light exposure. Likewise, direct comparison of values of $S_{\text{light}}(\lambda)$ at each exposure power in Fig. 9 cannot be undertaken (unlike Fig. 7) due to

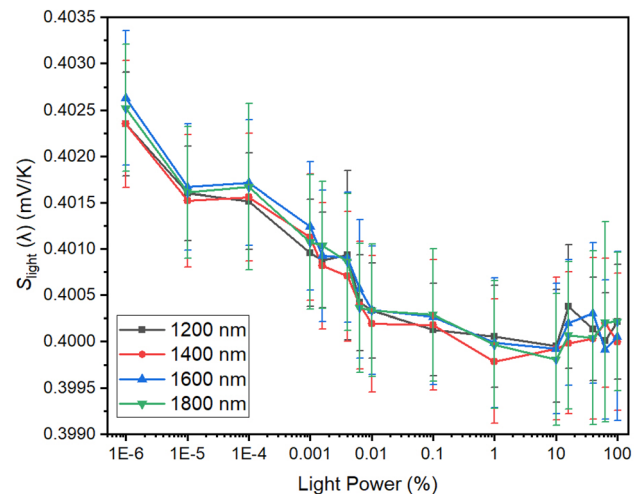


Fig. 9 Seebeck coefficient measured under selected monochromatic wavelengths as a function of illumination intensity

the experimental method. At the lowest light intensity, the Seebeck coefficient increases towards the dark value. It is of interest to note that the change in $S_{\text{light}}(\lambda)$ with increasing $I_0(\lambda)$ is seen to saturate for intensities greater than $\sim 0.1\%$ of that used to obtain the data shown in Figs. 7 and 8.

Finally, the photoconductivity of a-GeTe with respect to the intensity of light is presented in Fig. 10 obtained in the presence of the temperature gradient given ΔT . Upon illumination with light a photocurrent is observed which quickly saturates at $\sim 16\%$ of the maximum value of $I_0(\lambda)$ for $\Delta T = 15, 27$ and 41 °C. Prior to saturation of the photocurrent, its magnitude increases with reducing wavelength in line with the increase in absorption coefficient. The behaviour of the photocurrent measured for $\Delta T = 58$ °C displays a different behaviour, which is found to be reproducible, at values of $I_0(\lambda)$ above that which saturation is observed at lower values of ΔT . As $I_0(\lambda)$ is increased above this point ($\sim 16\%$) the photocurrent is found to decrease, with the effect being more prominent for wavelengths with a higher absorption coefficient. This behaviour is reversed again as the highest value of $I_0(\lambda)$ (100%) is reached.

4 Discussion

In the above description of the experimental behaviour of $S_{\text{light}}(\lambda)$ we turned to the detailed studies of a-GeTe and its proposed DOS to provide an initial

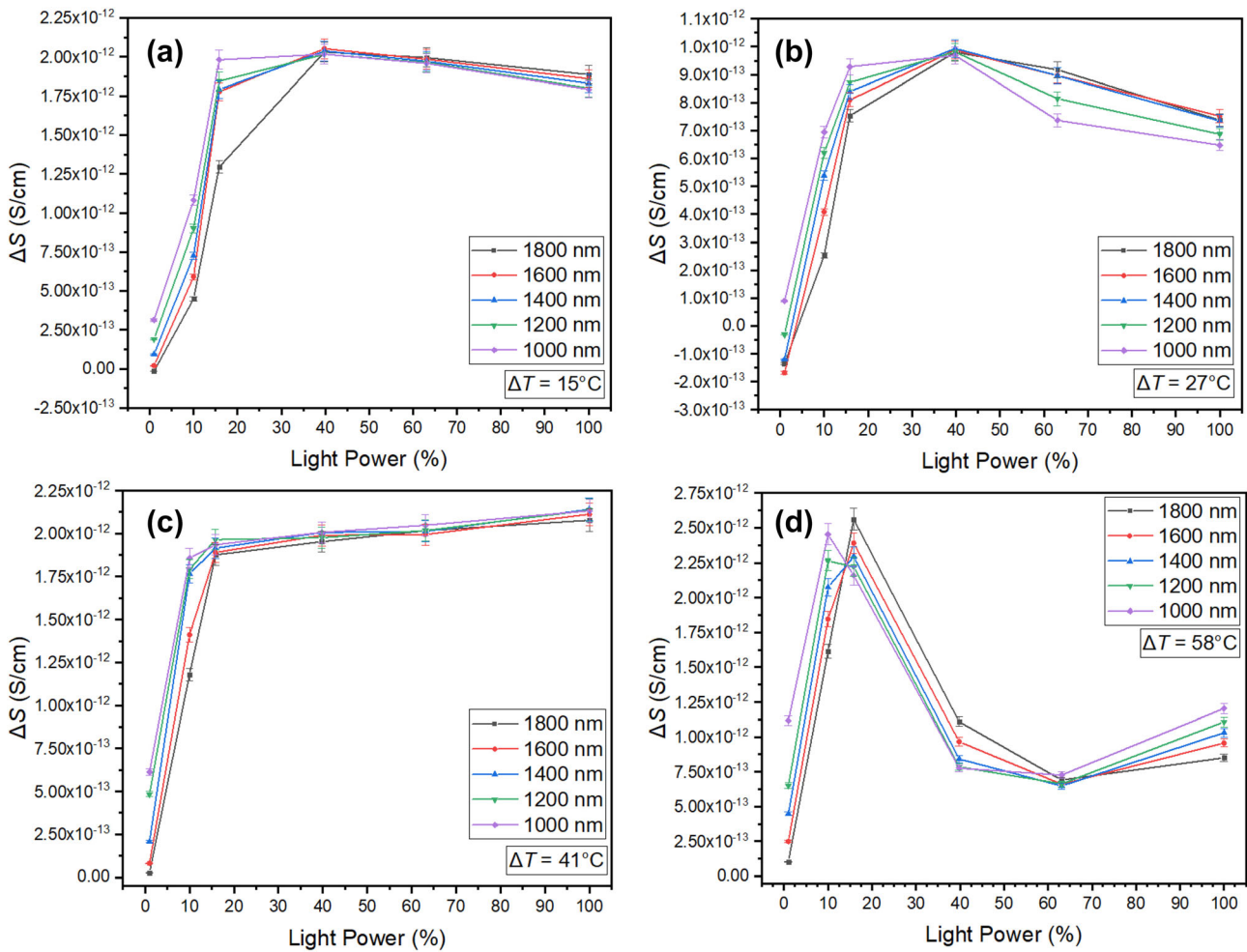


Fig. 10 Photoconductivity measurement of a-GeTe as function of light intensity and wavelength

interpretation of the observed spectrum. However, it is clear that the presence of oxygen within the film has modified the electrical properties. Firstly, we observe an increase in E_g from that reported for a-GeTe (~ 0.75 eV) [14] to ~ 0.88 eV in these a-GeTe-O systems. This is in agreement with ab initio molecular dynamics simulations [8] that show substitution of Te by O results in an increase in the bandgap of ~ 0.06 eV, whilst the formation of ‘dumbbell-like’ O- V_{Te} -Ge defects lead to an increase of ~ 0.08 eV. We note that such simulations typically underestimate the bandgap compared to experimental measurements hence a larger increase as observed within would not be unexpected. Additionally, the simulations are based on the incorporation of low O concentrations by the replacement of Te with O within the supercell, whereas in the material studied within a high O concentration was found during RBS analysis ($\sim 31\%$) with a similar Ge and

Te concentration ($\sim 34\%$ each). Previous studies of GeTe-O systems have suggested that at high ($> 10\%$) O concentration the formation of GeO_2 and TeO_2 crystals occurred [7]. We note that both of these materials are wide bandgap (> 3 eV) and therefore a thin film (100 nm) would be transparent whereas the film studied in our case remained dark brown/grey (Fig. 1).

It is also apparent that the presence of oxygen in these a-GeTe films reduces the value of $E_f - E_v$ from 0.31 eV in a-GeTe [14] to 0.16 eV in the studied a-GeTe-O system. This change is also reflected in the ab initio simulations [8] in the case of introducing O- V_{Te} -Ge defects where $E_f - E_v$ is significantly reduced. As such this then rules out the presence of a donor state centred at 0.25 eV above the valence band as found in a-GeTe. Nonetheless, the study of $V_{\text{light}}(\lambda)$ at energies within the bandgap (Fig. 8) does reveal evidence of optically active states with excitation

energies of ~ 0.1 eV and ~ 0.15 eV below E_g . The presence of O-V_{Te}-Ge defects, and also interstitial O, has been predicted to result in the formation of gap states which may be a source of such states.

The absorption of higher energy photons, for example 1.24 eV to 3 eV (400 nm to 1100 nm) has a significantly weaker effect (evidenced by a reduced gradient) than that at lower energies in the reduction of the Seebeck coefficient. This implies that excitation at very high energies with respect to the bandgap probably produces either more trapped electrons (which cannot diffuse or recombine with free holes) or electrons which quickly relax again into their original (ground) state before any diffusion or recombination can occur.

Upon further decrease in the energy of the photons towards the bandgap, the Seebeck voltages show some changes from 1 to 0.95 eV that may be due to the recombination of the excited electrons with the trapped holes. Considering the fact that the bottom of the conduction band is mostly formed from positively charged unoccupied p states [40], excitation into this state results in trapped electrons too. This follows the spectrum in Fig. 7 for the band to band excitation as the Seebeck coefficient shows more p-type behaviour. As the energy of incident photons is increased to be well above E_g (to ~ 1.24 eV) the dependency of $\Delta S(\lambda)$ again changes with three regions of varying behaviour being identified (Fig. 7).

5 Conclusion

The measurement of the photo-Seebeck coefficient of an amorphous semiconductor based on the direct measurement of the Seebeck voltage has been investigated. The Seebeck coefficients obtained under varying monochromatic light excitation showed that not only trap states are detectable using this technique, but there is also a potential of additional information such as the optical bandgap energy and an indication of the modification of carrier concentration and bonding arrangements of semiconductors due to light exposure. For example, the value of the bandgap for a-GeTe was determined using the photo-Seebeck spectrum of this sample. It is also noticed that this value is highly depended on the oxidation state of the device under test. The power dependence of the photo-Seebeck coefficient can be linked to variation in the carrier concentration of holes and

electrons upon absorption of light, and which was directly observed in the measurement of a-GeTe. Incident photons with lower energies than the optical bandgap interacts with the carriers within the sub-bandgap (either trap to band or band to trap) which directly affect the variation of the Seebeck coefficient. It is proposed that at higher excitation energies incident light produces more trapped electrons and/or electrons quickly relax to their original state. The changes in the photo-Seebeck spectra at higher energies are directly related to the bonding energies of the compounds. The variation of the Seebeck coefficient under influence of light is also depended on the structure of the amorphous chalcogenides which propose positively charged states that can interact with the excited or trapped electrons.

Acknowledgements

The authors would like to thank Dr Ioannis Zeimpekis and Dr Katrina Morgan for helpful discussions.

Funding

This work was supported in part by the Engineering and Physical Sciences Research Council (EPSRC) Grant EP/N020278/1.

Data Availability

The data that support the findings of this study are available upon request.

Compliance with ethical standards

Conflict of interest The authors declare that they have no conflicts of interest.

Open Access This article is licensed under a Creative Commons Attribution 4.0 International License, which permits use, sharing, adaptation, distribution and reproduction in any medium or format, as long as you give appropriate credit to the original author(s) and the source, provide a link to the Creative Commons licence, and indicate if changes were made. The images or other third party material in this article are included in the article's Creative Commons licence, unless indicated otherwise in a credit line to

the material. If material is not included in the article's Creative Commons licence and your intended use is not permitted by statutory regulation or exceeds the permitted use, you will need to obtain permission directly from the copyright holder. To view a copy of this licence, visit <http://creativecommons.org/licenses/by/4.0/>.

References

1. S.R. Ovshinsky, *Physical Properties of Amorphous Materials* (Springer, New York, 1985), p. 105
2. W. Matthias, Y. Noboru, *Nat. Mater.* **6**, 824 (2007)
3. S.R. Ovshinsky, *Phys. Rev. Lett.* **21**, 1450 (1968)
4. E.R. Meinders, *Optical Data Storage* (Springer, Dordrecht, 2006)
5. M. Chen, K.A. Rubin, R.W. Barton, *Appl. Phys. Lett.* **49**, 502 (1986)
6. E. Gourvest, B. Pelissier, C. Vallée, A. Roule, S. Lhostis, S. Maitrejean, *J. Electrochem. Soc.* **159**, H373 (2012)
7. X. Zhou, W. Dong, H. Zhang, R.E. Simpson, *Sci. Rep.* **5**, 11150 (2015)
8. L. Zhu, Z. Li, J. Zhou, N. Miao, Z. Sun, *J. Mater. Chem. C* **5**, 3592 (2017)
9. A.N. Kolb, N. Bernier, E. Robin et al., *ACS Appl. Electron. Mater.* **1**, 701 (2019)
10. X. Zhou, Y. Du, J.K. Behera, L. Wu, Z. Song, R.E. Simpson, *ACS Appl. Mater. Interfaces* **8**, 20185 (2016)
11. S.K. Bahl, K.L. Chopra, *J. Appl. Phys.* **40**, 4940 (1969)
12. S.K. Bahl, K.L. Chopra, *J. Appl. Phys.* **41**, 2196 (1970)
13. W.E. Howard, R. Tsu, *Phys. Rev. B* **1**, 4709 (1970)
14. C. Longeaud, J. Luckas, D. Krebs, R. Carius, J. Klomfass, M. Wuttig, *J. Appl. Phys.* **112**, 113714 (2012)
15. J. Luckas, S. Kremers, D. Krebs, M. Salinga, M. Wuttig, C. Longeaud, *J. Appl. Phys.* **110**, 013719 (2011)
16. J. Raty, W. Zhang, J. Luckas et al., *Nat. Commun.* **6**, 7467 (2015)
17. L. Shelimova, O. Karpinskii, P. Konstantinov, M. Kretova, E. Avilov, V. Zemskov, *Inorg. Mater.* **37**, 342 (2001)
18. Y. Gelbstein, O. Ben-Yehuda, E. Pinhas et al., *J. Electron. Mater.* **38**, 1478 (2009)
19. E. Levin, M. Besser, R. Hanus, *J. Appl. Phys.* **114**, 083713 (2013)
20. D. Wu, L.-D. Zhao, S. Hao et al., *J. Am. Chem. Soc.* **136**, 11412 (2014)
21. M. Samanta, T. Ghosh, R. Arora, U.V. Waghmare, K. Biswas, *J. Am. Chem. Soc.* **141**, 19505 (2019)
22. K. Chopra, S. Bahl, *Thin Solid Films* **12**, 211 (1972)
23. I. Dutsyak, *Tech. Phys.* **42**, 1035 (1997)
24. M.A. Hughes, Y. Fedorenko, B. Gholipour et al., *Nat. Commun.* **5**, 1 (2014)
25. M. Cagnoni, D. Führen, M. Wuttig, *Adv. Mater.* **30**, 1801787 (2018)
26. M. Grunewald, P. Thomas, D. Wurtz, *J. Phys. C* **14**, 4083 (1981)
27. M. Roilos, *Philos. Mag. B* **38**, 477 (1978)
28. J. Kakalios, *J. Non-Cryst. Solids* **114**, 372 (1989)
29. A.V. Kolobov, *J. Non-Cryst. Solids* **198**, 728 (1996)
30. J.G. Harper, H.E. Matthews, R.H. Bube, *J. Appl. Phys.* **41**, 765 (1970)
31. J.G. Harper, H.E. Matthews, R.H. Bube, *J. Appl. Phys.* **41**, 3182 (1970)
32. D.I. Jones, F. Goesmann, *J. Non-Cryst. Solids* **198**, 210 (1996)
33. M. Wang, C. Bi, L. Li et al., *Nat. Commun.* **5**, 4598 (2014)
34. K. Tanabe, *J. Appl. Phys.* **124**, 143902 (2018)
35. P.S. Mondal, R. Okazaki, H. Taniguchi, I. Terasaki, *J. Appl. Phys.* **116**, 193706 (2014)
36. M. Mayer, *SIMNRA User's Guide* (Max-Planck-Institut für Plasmaphysik Garching, München, 1997)
37. A.M. Shing, Y. Tolstova, N.S. Lewis, H.A. Atwater, *Appl. Phys. A* **123**, 735 (2017)
38. S.O. Kasap, *Principles of Electronic Materials and Devices* (McGraw-Hill, New York, 2006)
39. N. Shevchik, J. Tejada, D. Langer, M. Cardona, *Physica Status Solidi (b)* **57**, 245 (1973)
40. T. Takahashi, H. Sakurai, T. Sagawa, *Solid State Commun.* **44**, 723 (1982)

Publisher's Note Springer Nature remains neutral with regard to jurisdictional claims in published maps and institutional affiliations.